JOURNAL

OF THE AMERICAN CHEMICAL SOCIETY

VOLUME 106, NUMBER 15 JULY 25, 1984

Dynamics of Ion–Molecule Recombination. 3. Trends in the Recombination Efficiency†

Kandadai N. Swamy and William L. Hase*

Contribution from the Department of Chemistry, Wayne State University, Detroit, Michigan 48202. *Received December 12, 1983*

Abstract: The quasiclassical trajectory method is used to study the dynamics of ion–molecule recombination reactions. Recombination cross sections are calculated as a function of the initial relative translational energy. The following trend is found for the efficiency of ion–molecule recombination: $K^+ + H_2O < Na^+ + H_2O < Li^+ + H_2O < Li^+ + D_2O < Li^+(H_2O) + H_2O < Li^+ + (CH_3)_2O$. As the relative translational energy is increased, significant differences are found between the quasiclassical trajectory recombination cross sections and those predicted by the ADO and AMI theories. A short discussion is given of the details for an ion–molecule recombination dynamical model. The ADO, AMI, and quasiclassical trajectory rate constants are compared at 300 K.

I. Introduction

An understanding of the dynamics and kinetics of ion–molecule recombination reactions will lead to more knowledge about different chemical phenomena. Ion–molecule recombination reactions are important for bimolecular processes which are direct and those which proceed through long-lived collision complexes.[1-8] They are also elementary steps in solvation and the formation of clusters.[9-14] Information about the dynamics and kinetics of ion–water molecules association will assist in interpreting the changes in the properties of an ion–molecule reaction as its environment undergoes a transition from the gas to liquid phase.[15,16]

Different models have been developed for calculating the ion–molecule recombination rate constant. Most assume that the long-range forces control the recombination kinetics as in the Langevin collisional model where the charge-induced dipole potential

$$V(r) = -\alpha q^2/2r^4 \qquad (1)$$

is used. In the average dipole orientation (ADO) collisional model of Su and Bowers,[17] as refined by Bates,[18,19] the $-(q\mu_D/r^2)\cos\theta$ term representing the ion–dipole interaction is added to $V(r)$ in eq 1. For these collisional models it is postulated that orbital angular momentum is conserved until recombination occurs, and the resulting centrifugal potential gives rise to the barrier for recombination. Another approach is to use the same potential functions as for the collisional models, but to calculate the recombination rate constant with variational transition-state theory.[20,21]

The above models have received some success in direct comparisons of calculated and experimental rate constants, and in correlating experimental rate constants.[17,20] However, they have limitations. The assumed potential energy functions are quite simple. They neglect anisotropies in the intermolecular potentials as well as the effect of the intramolecular potential. These may be important considerations. Also, crucial assumptions like those of transition-state theory are made.[22,23]

† This research was presented in part at the 184th National Meeting of the American Chemical Society, Kansas City, MO, 1982.

(1) W. N. Olmstead, M. Lev-On, D. M. Golden, and J. I. Brauman, *J. Am. Chem. Soc.*, **99**, 992 (1977).
(2) W. N. Olmstead and J. I. Brauman, *J. Am. Chem. Soc.*, 99, 4219 (1977).
(3) M. J. Pellerite and J. I. Brauman, *J. Am. Chem. Soc.*, **102**, 5993 (1980).
(4) W. J. Chesnavich, T. Su, and M. T. Bowers, *J. Am. Chem. Soc.*, **100**, 4362 (1978).
(5) L. Bass, W. J. Chesnavich, and M. T. Bowers, *J. Am. Chem. Soc.*, **101**, 5493 (1979).
(6) L. M. Bass, P. R. Kemper, V. G. Aricich, and M. T. Bowers, *J. Am. Chem. Soc.*, **103**, 5283 (1981).
(7) W. J. Chesnavich, L. Bass, T. Su, and M. T. Bowers, *J. Chem. Phys.*, 74, 2228 (1981); M. F. Jarrold, L. M. Bass, P. R. Kemper, P. A. M. van Koppen, and M. T. Bowers, *ibid.*, **78**, 3756 (1983).
(8) R. L. Woodin and J. L. Beauchamp, *Chem. Phys.*, **41**, 1 (1979).
(9) J. Q. Searcy and J. B. Fenn, *J. Chem. Phys.*, **61**, 5282 (1974).
(10) A. W. Castleman, Jr., P. M. Holland, D. M. Lindsay, and K. I. Peterson, *J. Am. Chem. Soc.*, **100**, 6039 (1978).
(11) A. W. Castleman, Jr., *Chem. Phys. Lett.*, **53**, 506 (1978).
(12) A. W. Castleman, Jr., *Adv. Colloid Interface Sci.*, **10**, 73 (1979).
(13) A. W. Castleman, Jr., *Radiat. Phys. Chem.*, **20**, 57 (1982).
(14) Y. K. Lau, S. Ikuta, and P. Kebarle, *J. Am. Chem. Soc.*, **104**, 1462 (1982).
(15) D. K. Bohme and G. I. Mackay, *J. Am. Chem. Soc.*, **103**, 978 (1981).
(16) R. T. McIver, Jr., *Sci. Am.*, **243**, 186 (1980).
(17) T. Su and M. T. Bowers in "Gas Phase Ion Chemistry", Vol. 1, M. T. Bowers, Ed., Academic Press, New York, 1979, p 83; T. Su and M. T. Bowers, *J. Chem. Phys.*, **58**, 131 (1973).
(18) D. R. Bates, *Chem. Phys. Lett.*, **82**, 396 (1981); D. R. Bates, *Proc. R. Soc. London, Ser. A 384*, 289 (1982).
(19) D. R. Bates, *Chem. Phys. Lett.*, 97, 19 (1983).
(20) W. J. Chesnavich and M. T. Bowers in ref 17, p 119.
(21) W. J. Chesnavich, T. Su, and M. T. Bowers, *J. Chem. Phys.*, **72**, 264 (1980).
(22) D. G. Truhlar and B. C. Garrett, *Acc. Chem. Res.*, **13**, 440 (1980).
(23) W. L. Hase, *Acc. Chem. Res.*, **16**, 258 (1983).

0002-7863/84/1506-4071$01.50/0

In recent work ab initio[24-28] and semiempirical[29-32] potential energy surfaces have been derived for ion–molecule interactions. The collisional and transition-state models could be applied to these surfaces. However, this would require a major effort since these potential energy surfaces are considerably more complex than the simple models described above. A particularly troublesome problem in applying transition-state theory is the treatment of the transition of reactant rotational degrees of freedom to first anharmonic librational motion and then anharmonic vibrational motions.

Ion–molecule recombination is an ideal reaction for the application of the quasiclassical trajectory method.[33-35] Since the activated complex has an early location along the reaction path, accurate quantization of reactant vibrational motions will result in a correct treatment of adiabaticity for these motions in the entrance channel. Also, there is no potential energy barrier and quantum mechanical tunneling is unimportant. Formation of a vibrationally excited ion–molecule complex occurs upon energy transfer from relative translation to vibrational and/or rotational motions of the complex. Owing to the large density of states involved, classical mechanics is expected to correctly describe the probability for this transition.

Quasiclassical trajectory calculations have provided important information about ion–molecule reactions.[31,32,36-39] In addition to giving accurate rate constants, the trajectory calculations furnish valuable microscopic details about the recombination dynamics. In parts I and II of this series[38,39] quasiclassical trajectories were used to study the dynamics of $Li^+ + H_2O$, D_2O and $K^+ + H_2O$ recombination. An important finding of these studies is that alkali ion–water molecular collisions exhibit properties of weakly interacting systems. As a result the recombination rate constants are smaller than those calculated from the model collisional and transition-state theories described above. In the work presented here the related but significantly different systems $Na^+ + H_2O$, $Li^+(H_2O) + H_2O$, and $Li^+ + (CH_3)_2O$ have been studied. A major goal is to determine how different intermolecular and intramolecular potential energy surfaces affect the recombination dynamics.

II. Potential Energy Surfaces

The general form for the analytic potential energy surface used in the trajectory calculations is

$$V = V_{inter} + V_{intra} + V^0 \quad (2)$$

V_{intra} is the sum of the intramolecular potentials for the reactant molecules, V_{inter} is the intermolecular potential between the reactant molecules, and V^0 is chosen to make the potential energy equal to zero at the lowest minimum on the surface and it is equal to the ion–molecule binding energy.

Table I. Equilibrium Properties of the Alkali Ion–Water Molecule Potential Energy Surfaces

property[a]	H_2O	$Li^+(H_2O)$	$Na^+(H_2O)$	$K^+(H_2O)$
r^0	0.957	0.985	0.977	0.971
θ^0	104.5	94.4	96.2	97.9
R^0		1.82	2.17	2.59
V^0		37.2	26.9	18.4
H_2O bend[b]	1659	1861	1832	1798
OH sym st.	3807	3479	3568	3643
OH asym st.	3942	3585	3678	3757
I^+–O st.		529	455	390
I^+–H_2O in-plane bend		523	357	252
I^+H_2O out-of-plane bend		594	496	451

[a] Distances are in Å, angles in deg, potential energy in kcal/mol, and frequencies in cm^{-1}. The internal coordinates are defined in parts I and II. [b] Harmonic vibrational frequencies are listed.

Table II. Equilibrium Properties of the $Li^+ + (CH_3)_2O$ Potential Energy Surface[a]

property	$(CH_3)_2O$	$Li^+[(CH_3)_2O]$	$(CH_3)_2O'$[c]	$Li^+[(CH_3)_2O']$
R^0		1.68		1.69
V^0		34.8		34.4
Harmonic Vibrational Frequencies[b]				
	2975	2950	3092	3077
	2971	2947	2978	2959
	2970	2936	2978	2945
	2969	2936	2977	2945
	2858	2830	2896	2865
	2858	2830	2887	2860
	1618	1632	2464	2482
	1603	1624	2361	2364
	1454	1454	2142	2140
	1448	1441	1897	1913
	1438	1432	1897	1894
	1429	1427	1817	1822
	1211	1266	1710	1702
	1180	1205	1707	1690
	1169	1127	1388	1396
	1130	1085	1345	1341
	1034	1034	1337	1307
	905	958	1307	1296
	440	641	1073	1105
		422		625
		162		168
		132		98

[a] Distances are in Å, potential energy in kcal/mol, and frequencies in cm^{-1}. [b] The two internal rotors are free rotors. [c] $(CH_3)_2O'$ is the tight model for dimethyl ether; see text.

A. Li^+, Na^+, $K^+ + H_2O$, D_2O Potential. For the alkali ion–water molecule trajectory calculations the anharmonic intramolecular potential is denoted by V^{anh}_{intra}. The form of the potential and its parameters are given in part I.[38] Switching functions and valence internal coordinates are used to match the H_2O and OH equilibrium geometries, harmonic frequencies, and dissociation energies. As shown in part I the trajectory results are rather insensitive to the exact form of the intramolecular potential, since a harmonic potential V^{har}_{intra} gives the same results as does V^{anh}_{intra}.[40]

The alkali ion–water molecule intermolecular potential is called V^{ll}_{inter}. As described in part II, it is a fit by Kistenmacher et al.[25] to ab initio calculations and is written as a sum of two-body interactions. Interaction centers are located on the atoms, at the midpoints of the OH bonds, and along the bisector of the HOH angle. The potential gives an excellent fit to the experimental alkali ion–water molecule binding energies. Properties of the alkali

(24) E. Clementi and H. Popkie, *J. Chem. Phys.*, **57**, 1077 (1972).
(25) H. Kistenmacher, H. Popkie, and E. Clementi, *J. Chem. Phys.*, **59**, 5842 (1973); D. G. Bounds and P. J. Bounds, *Mol. Phys.*, **50**, 25 (1983).
(26) G. Corongiu, E. Clementi, E. Pretsch, and W. Simon, *J. Chem. Phys.*, **70**, 1266 (1979).
(27) G. Corongiu, E. Clementi, E. Pretsch, and W. Simon, *J. Chem. Phys.*, **72**, 3096 (1980).
(28) E. Clementi, G. Corongiu, and G. Ranghino, *J. Chem. Phys.*, 74, 578 (1981).
(29) P. Perez, W. K. Lee, and E. W. Prohofsky, *J. Chem. Phys.*, 79, 388 (1983).
(30) B. T. Gowda and S. W. Benson, *J. Chem. Phys.*, **79**, 1235 (1983).
(31) F. H. Stillinger and T. A. Weber, *Chem. Phys. Lett.*, **79**, 259 (1981); T. A. Weber and F. H. Stillinger, *ibid.*, **89**, 154 (1982).
(32) T. A. Weber and F. H. Stillinger, *J. Chem. Phys.*, **77**, 4150 (1982).
(33) D. L. Bunker, *Methods Comput. Phys.*, **10**, 287 (1971).
(34) R. N. Porter and L. M. Raff "Modern Theoretical Chemistry", Vol. 2, "Dynamics of Molecular Collisions", Part B, W. H. Miller, Ed., Plenum Press, New York, 1976, p 1.
(35) D. G. Truhlar and J. T. Muckerman in "Atom-Molecule Collision Theory: A Guide for the Experimentalist", R. B. Bernstein, Ed., Plenum, New York, 1979, p 505.
(36) D. Gerlich, U. Nowotny, Ch. Schlier, and E. Teloy, *Chem. Phys.*, **47**, 245 (1980).
(37) L. M. Babcock and D. L. Thompson, *J. Chem. Phys.*, **78**, 2394 (1983).
(38) Part I: W. L. Hase and D.-F. Feng, *J. Chem. Phys.*, **75**, 738 (1981).
(39) Part II: K. N. Swamy and W. L. Hase, *J. Chem. Phys.*, **77**, 3011 (1982).

(40) Though the intramolecular potential energy is harmonic and separable for V^{har}_{intra}, the intramolecular Hamiltonian is nonseparable owing to kinetic energy coupling terms.

ion–water molecule potential energy surfaces are given in Table I.

B. $Li^+ + (CH_3)_2O$ Potential. The dimethyl ether intramolecular potential is written in terms of internal coordinates with the bends represented by harmonic oscillators and the stretches by Morse oscillators:

$$V_{intra}^{har,M} = \sum_{CH\ sts} D_{CH}[1 - e^{-\beta_{CH}(r-r^0_{CH})}]^2 + \sum_{CO\ sts} D_{CO}[1 - e^{-\beta_{CO}(r-r^0_{CO})}]^2 + \sum_{HCH\ bends} \tfrac{1}{2} f_{HCH}(\theta - \theta^0_{HCH})^2 + \sum_{HCO\ bends} \tfrac{1}{2} f_{HCO}(\theta - \theta^0_{HCO})^2 + \tfrac{1}{2} f_{COC}(\theta - \theta^0_{COC})^2 \quad (3)$$

The values for the parameters are D_{CH} = 104.0 kcal/mol, D_{CO} = 81.0 kcal/mol, β_{CH} = 1.801 Å^{-1}, β_{CO} = 2.127 Å^{-1}, f_{HCH} = 0.508 mdyn·Å/rad^2, f_{HCO} = 0.880 mdyn·Å/rad^2, and f_{COC} = 1.313 mdyn·Å/rad^2. The equilibrium geometry used for dimethyl ether was determined from microwave spectra by Blukis et al.[41] The two internal rotors of dimethyl ether are treated as free rotors.[42]

The lithium ion–dimethyl ether intermolecular potentials was derived by Corongiu et al. from ab initio calculations[27] and is referred to here as V_{inter}^{III}. It is expressed as the following sum of two-body terms:

$$V_{inter}^{III} = \sum_i (-A_{iM}/r_{iM}^6 + B_{iM}/r_{iM}^{12} + C_{iM}q_iq_M/r_{iM}) \quad (4)$$

where the r_{iM} are the distances between Li$^+$(M) and the atoms (i) of dimethyl ether. The values used for A_{iM}, B_{iM}, C_{iM}, q_i, and q_M are those given by Corongiu et al.[27] Properties of the $Li^+ + (CH_3)_2O$ potential energy surface are listed in Table II. The lithium ion–dimethyl ether complex has C_{2v} symmetry with Li$^+$ attached to the oxygen atom. The binding energy of 34.8 kcal/mol agrees with the experimental value of ~38 kcal/mol.[27] Frequencies for the three modes formed by the $Li^+ + (CH_3)_2O$ interaction are Li$^+$–O stretch, 641 cm^{-1}; Li$^+$–$(CH_3)_2O$ in-plane bend, 162 cm^{-1}; and Li$^+$–$(CH_3)_2O$ out-of-plane bend, 132 cm^{-1}.

A model with higher vibrational frequencies for dimethyl ether is also considered. It is called the tight dimethyl ether model and denoted by $(CH_3)_2O'$. For this model the bending force constants are raised to f_{HCH} = 0.508 mdyn·Å/rad^2, f_{HCO} = 2.0 mdyn·Å/rad^2, and f_{COC} = 16.0 mdyn·Å/rad^2.

C. $Li^+(H_2O) + H_2O$ Potential. The potential energy function for a lithium ion and two water molecules is a sum of two H_2O intramolecular potentials, two $Li^+ + H_2O$ intermolecular potentials, and a $H_2O + H_2O$ intermolecular potential. The H_2O intramolecular potential is like that used for $(CH_3)_2O$ (eq 3). There are two Morse oscillators with D = 125.6 kcal/mol, β = 2.194 Å^{-1}, and r^0 = 0.957 Å; and a harmonic bend with f = 0.688 mdyn·Å/rad^2 and θ^0 = 104.5°.

V_{inter}^{I}, which is described in part I,[38] is used for the $Li^+ + H_2O$ intermolecular potential. The addition of another water molecule to the system considerably complicates the potential energy surface, and V_{inter}^{I} is used here instead of V_{inter}^{II} since it is simpler in form and has fewer terms. Which of these two intermolecular potentials is used is not of crucial concern. They give similar results for the $Li^+ + H_2O \rightarrow Li^+(H_2O)$ recombination dynamics,[39] and the same finding is expected when another H_2O molecule is added to the system.

The water–water intermolecular interaction is represented by the analytic ab initio potential of Lie and Clementi,[43] which includes a dispersion correction obtained from perturbation calculations. This potential has been used in a Monte Carlo simulation of liquid water and the results are in good agreement with experiment.[43]

Various equilibrium properties of the $Li^+(H_2O) + H_2O$ potential energy surface are listed in Table III. The $Li^+(H_2O)_2$ complex has C_{2v} symmetry with the O–Li–O atoms forming a straight line. The two water molecules have a staggered configuration.

Table III. Equilibrium Properties of the $Li^+(H_2O) + H_2O$ Potential Energy Surface[a]

property	$Li^+(H_2O)$	$Li^+(H_2O)_2$
R^0	1.85	1.86
V^0	34.6	66.6
Harmonic Vibrational Frequencies		
	3737	3760 (2)
	3702	3727
	1677	3716
	558	1679
	547	1667
	473	693
		550 (2)
		449 (2)
		281
		58
		40 (2)

[a] Distances are in Å, potential energy in kcal/mol, and frequencies in cm^{-1}.

III. Quasiclassical Trajectory Calculations

A. Initial Conditions and Numerical Integrations. The quasiclassical trajectory calculations were performed with our general computer program MERCURY.[44] The analytic functions described above are standard options in this computer program. Initial conditions for the trajectories were chosen to simulate random collisions between an ion and a molecule. The molecule is randomly oriented with respect to the ion, and an impact parameter b is chosen randomly according to the distribution

$$P(b) = 2b/b_m^2 \qquad b \le b_m \qquad P(b) = 0 \qquad b > b_m \quad (5)$$

The maximum impact parameter b_m that leads to reaction was deduced by tests.

The initial relative translational energy E_{rel} was varied in the calculations. The initial values for vibrational energy E_{vib} and rotational energy E_{rot} were kept constant. Zero-point energy is added to each vibrational degree of freedom. A 300-K rotational energy distribution is added to the molecules and polyatomic ions using the algorithm described by Bunker and Goring-Simpson.[45] In part II it was found that the recombination cross sections are insensitive to the rotational energy for T_{rot} in the range 0–1000 K. The initial separation between the ion and the molecule was chosen so that only a negligible and unimportant intermolecular interaction existed.[38,39]

The trajectories were performed on an Amdahl 470V/6 computer and a VAX11/780 computer. A fixed integration time step of 2.00×10^{-16} s, chosen by backward integration tests, was used in the calculations.

B. Criterion for Recombination. The recombination of an ion and a molecule leads to the formation of a vibrationally and rotationally excited collision complex:

$$I^+ + M \rightarrow I^+(M)^* \quad (6)$$

Stabilization of the complex occurs by emission of electromagnetic radiation or by collision with a bath molecule. The former usually occurs on a 10^{-6} s or longer time scale. Complexes with shorter lifetimes can be stabilized by collisions.

We have used the following phenomenological approach to classify trajectories as complex forming. In order to form the complex, the initial relative translational energy of the ion–molecule collision must be transferred to the complex's vibrational and/or rotational degrees of freedom. This will give rise to a collision complex which can be identified by the presence of multiple inner turning points in the I$^+$—M relative distance. If

(41) U. Blukis, P. H. Kasai, and R. J. Myers, *J. Chem. Phys.*, **38**, 2753 (1963).
(42) P. Groner and J. R. Durig, *J. Chem. Phys.*, **66**, 1856 (1977).
(43) G. C. Lie and E. Clementi, *J. Chem. Phys.*, **62**, 2195 (1975).
(44) W. L. Hase, *QCPE*, **3**, 453 (1983).
(45) D. L. Bunker and E. A. Goring-Simpson, *Discuss. Faraday Soc.*, **55**, 93 (1973).

Table IV. Comparison of Primary Reactive Cross Sections

system[a]	cross section ($Å^2$)[c] at E_{rel}[b] = 0.5	1.0	2.0	3.0	4.0	5.0	6.0	7.0	10.0	15.0
$Li^+ + H_2O$	347 ± 48	172 ± 28	55 ± 11	30 ± 7	11 ± 4	7.5 ± 3.3	0.0[g]	...[h]	...	...
$Li^+ + D_2O$	386 ± 54	305 ± 29	126 ± 15	52 ± 9	31 ± 6	13 ± 4	5.7 ± 2.5	4.5 ± 2.2	...	...
$Na^+ + H_2O$[d]	238 ± 46	70 ± 16	19 ± 8	4.0 ± 2.8	...	...	...	...	...	...
$K^+ + H_2O$[e]	216 ± 45	69 ± 15	4.6 ± 2.6	...	...	...	...	...	...	...
$Li^+ + (CH_3)_2O$	...	489 ± 59	...	163 ± 25	...	134 ± 18	...	103 ± 12	64 ± 11	33 ± 6
$Li^+ + (CH_3)_2O'$[f]	...	461 ± 59	...	199 ± 26	...	93 ± 16	...	75 ± 11	16 ± 6	12 ± 4
$Li^+(H_2O) + H_2O$	629 ± 86	386 ± 40	...	227 ± 17	...	88 ± 14	...	64 ± 11	53 ± 8	11 ± 3

[a] The reactant molecules and polyatomic ions have a 300 K rotational energy distribution. Each vibrational degree of freedom contains zero-point energy. [b] Initial relative translational energy in kcal/mol. [c] The error in the cross section is for one standard deviation. [d] The $Na^+ + H_2O$ cross section is 33 ± 11 $Å^2$ at 1.5 kcal/mol and 8.4 ± 4.1 $Å^2$ at 2.5 kcal/mol. [e] The $K^+ + H_2O$ cross section is 16 ± 8 $Å^2$ at 1.5 kcal/mol and 6.3 ± 3.6 Å at 2.5 kcal/mol. [f] $(CH_3)_2O'$ is the tight model for dimethyl ether; see text. [g] No reactions occurred out of 50 trajectories. [h] (...) means the calculation was not performed.

this energy transfer process is inefficient, there will only be one inner turning point, and the ion–molecule collision will resemble that between two monatomic species. The collision time for such events is of the order of 10^{-13} s or less.

In this work we report the primary reactive cross section σ, which is the cross section for forming ion–molecule collision complexes with two or more inner turning points in the I^+—M distance. It is expected that the deactivation of these complexes can be treated by an uncorrelated collisional model as is used in RRKM theory.[39,46] On the other hand, the collision time for events with only one inner turning point is so short that these events can only be intercepted by deactivating collisions at ultrahigh pressures or in a condensed medium. Under these conditions the collisional events become correlated and the treatment of collisions used in RRKM theory becomes inappropriate.

The cross section σ is the complex forming reactive cross section in the high-pressure limit for uncorrelated collisions. At lower pressures decomposition of the complex occurs and the observed cross section is referred to as the secondary reactive cross section σ_s.[39] By integrating the trajectories for longer times to determine the lifetime distribution of the collision complex, it is possible to estimate σ_s as a function of pressure. However, for some situations there are problems in using classical trajectories to compute unimolecular lifetimes. This arises from the fact that dissociating molecules can classically attain the transition-state configuration without zero-point energy in the degrees of freedom orthogonal to the reaction coordinate.[47] In this work only a few preliminary studies were undertaken to determine dissociation probabilities of the ion–molecule collision complexes. For the $Na^+(H_2O)$ collision complex there is a high dissociation probability after two inner turning points as was found for the $Li^+(H_2O)$ collision complex.[39] In contrast, dissociation of the $Li^+(CH_3)_2O$ collision complex is not observed. As discussed below, a strongly non-statistical dissociation process is found for the $Li^+(H_2O)_2$ complex.

IV. Recombination Cross Sections

A. Quasiclassical Trajectory Results. Listed in Table IV are the trajectory primary reactive cross sections determined in the previous trajectory studies and in the work presented here. For a large initial relative translational energy, recombination is seen to be most efficient for $Li^+ + (CH_3)_2O$ and $Li^+(H_2O) + H_2O$. There are two significant trends in the ion–molecule recombination cross sections, and they are illustrated in Figures 1 and 2 where ln σ is plotted vs. E_{rel}. Figure 1 shows the effect of changing the ion but not changing the molecule, H_2O. The interaction between K^+ and H_2O is the weakest and is the most long range. This is the most probable explanation for the finding that K^+ is the least efficient ion for recombination. Though $Li^+(H_2O) + H_2O$ and $Li^+ + H_2O$ have nearly equal intermolecule well depths, $Li^+(H_2O)$ is expected to be the more efficient ion for recombination since the low-frequency $Li^+(H_2O)$ vibrations should easily absorb the initial relative translational energy and facilitate recombination.

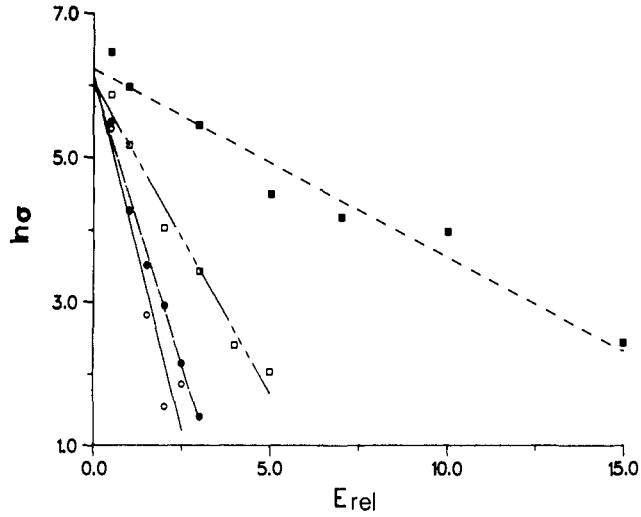

Figure 1. Plot of the natural logarithm of the recombination cross section in $Å^2$ vs. E_{rel}(kcal/mol) for $K^+ + H_2O$ (—), $Na^+ + H_2O$ (– – –), $Li^+ + H_2O$ (– · – · –), and $Li^+(H_2O) + H_2O$ (– · · –). The trajectory results are given by ○, ●, □, and ■ for $K^+ + H_2O$, $Na^+ + H_2O$, $Li^+ + H_2O$, and $Li^+(H_2O) + H_2O$, respectively.

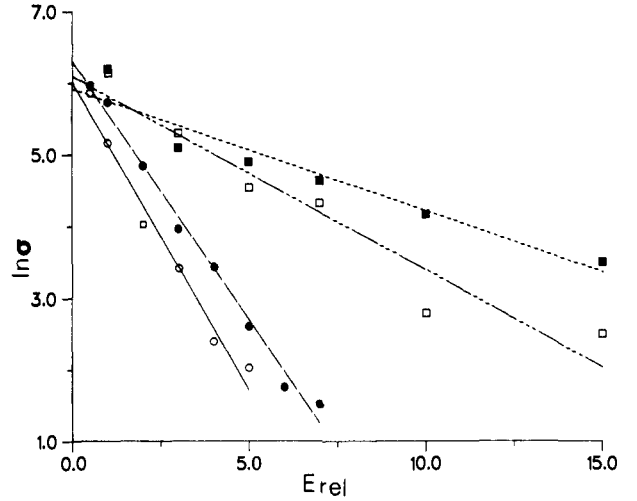

Figure 2. Plot of the natural logarithm of recombination cross section in $Å^2$ vs. E_{rel} (kcal/mol) for $Li^+ + H_2O$ (—), $Li^+ + D_2O$ (– – –), $Li^+ + (CH_3)_2O'$ (– · – · –), and $Li^+ + (CH_3)_2O$ (– · · –). The trajectory results are given by ○, ●, □, and ■ for $Li^+ + H_2O$, $Li^+ + D_2O$, $Li^+ + (CH_3)_2O'$, and $Li^+ + (CH_3)_2O$, respectively.

The trend observed when the molecule is varied is depicted in Figure 2. Water is the least efficient and dimethyl ether is the most efficient. This difference is most likely due to the internal rotations and low-frequency vibrations present in $(CH_3)_2O$, but not in H_2O. This interpretation is supported by the lower recombination efficiency for the tight $(CH_3)_2O$ model as compared

(46) D. L. Bunker, *J. Chem. Phys.*, *40*, 1946 (1964); W. Forst, Theory of Unimolecular Reactions, Academic Press, New York, 1973, p 151; W. L. Hase in ref 34, p 121.

(47) W. L. Hase and D. G. Buckowski, *J. Comput. Chem.*, 3, 335 (1982).

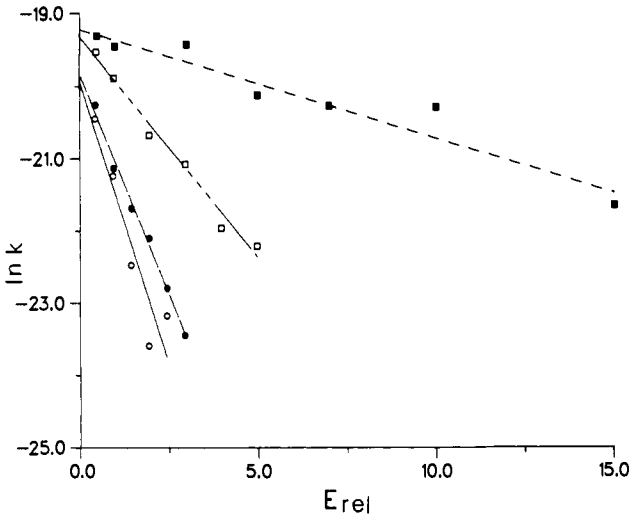

Figure 3. Same as Figure 1 but the natural logarithm of $k(E_{rel})$ is plotted. $k(E_{rel})$ is in units of cm^3/molecule s.

Table V. Parameters for the Energy Dependence of the Recombination Cross Sections and Rate Constants[a,b]

reaction	a	b	a'	b'
$K^+ + H_2O$	440.32	1.96	229.92	1.56
$Na^+ + H_2O$	407.71	1.56	249.28	1.22
$Li^+ + H_2O$	409.02	0.86	397.91	0.61
$Li^+ + D_2O$	542.43	0.72	581.31	0.54
$Li^+(H_2O) + H_2O$	498.10	0.26	447.14	0.15
$Li^+ + (CH_3)_2O$	371.50	0.17	538.16	0.08

[a] a is in units of Å^2 and b in units of (kcal/mol)$^{-1}$. [b] a' is in units of 10^{-11} cm^3/molecules and b' in units of (kcal/mol)$^{-1}$.

with the normal model. Thus, the "softer" and/or "floppier" ions and molecules which have the low-frequency vibrations recombine the most efficiently.

In our earlier studies[38,39] it was found that the expression

$$\sigma(E_{rel}) = a \exp(-bE_{rel}) \tag{7}$$

gives an excellent fit to the trajectory recombination cross sections for values of E_{rel} greater than or equal to one. We have not been able to derive this expression from a dynamical model for the recombination reaction. As shown in Figure 1 and 2 it tends to underestimate the trajectory cross sections at $E_{rel} = 0.50$ kcal/mol. In this work it was discovered that the analytic expression for the microscopic recombination rate constant

$$k(E_{rel}) = a' \exp(-b'E_{rel}) \tag{8}$$

yields a better fit to the trajectory results at the lower relative translational energies. This is shown in Figure 3 for the recombination of different ions with the water molecule. Values of the parameters a and b in eq 7 and a' and b' in eq 8 are given in Table V.

B. Comparison of Quasiclassical Trajectory Cross Sections with Those of ADO and AMI Theory. Recombination cross sections for $Li^+ + H_2O$ and $Li^+ + (CH_3)_2O$ are calculated with the Su–Bowers average dipole orientation (ADO) theory[17,48] and with the average molecular interaction (AMI) theory.[39] They are compared with the trajectory cross sections in Table VI. The ADO and AMI cross sections for the reactions are nearly identical over the complete energy range. The similarity between these theories has been discussed previously.[39] At low initial relative translational energies there is good agreement between the trajectory cross sections and those calculated with the ADO and AMI theories for each of the reactions. As the energy is increased the trajectory and model theory cross sections still agree for $Li^+ + (CH_3)_2O$. However, for $Li^+ + H_2O$ the trajectory cross sections become

Table VI. Trajectory and Model Theory Recombination Cross Sections

		recombination cross section (Å^2)		
E_{rel}[a]	reaction[b]	trajectory	ADO theory[c]	AMI theory[c]
0.5	A	347 ± 48	347.2	568.4
	B		352.8	477.5
1.0	A	172 ± 28	213.2	368.4
	B	489 ± 59	245.4	324.6
2.0	A	55 ± 11	129.7	224.9
	B		166.1	215.7
3.0	A	30 ± 7	97.5	165.6
	B	163 ± 25	131.7	168.5
4.0	A	11 ± 4	80.0	133.0
	B		111.7	141.2
5.0	A		68.8	112.3
	B	134 ± 18	98.4	123.0
7.0	A		55.0	87.0
	B	103 ± 12	81.4	100.0
10.0	A		43.6	66.6
	B	64 ± 11	66.7	80.4
15.0	A		33.7	49.5
	B	33 ± 6	53.3	62.9

[a] E_{rel} is in units of kcal/mol. [b] Reaction A is $Li^+ + H_2O$; reaction B is $Li^+ (CH_3)_2O$. [c] The temperature used in the ADO and AMI theory calculations is the rotational temperature of 300 K.

significantly smaller. This is a result of the inefficient energy transfer for $Li^+ + H_2O$ collisions at the high initial relative translational energies.

C. $Li^+(H_2O) + H_2O \rightarrow H_2O + Li^+(H_2O)$ Displacement Channel. In the trajectory calculations for $Li^+(H_2O) + H_2O$ a direct displacement reactive channel was observed in addition to recombination. For the direct displacement trajectories it is found that once two inner turning points occur between the adding water and Li^+, this water molecule does *not* dissociate within a lifetime that spans six inner turning points in its relative motion with Li^+.[49] However, the H_2O molecule initially bound to Li^+ does dissociate. There are two mechanisms for this dissociation. The first, which becomes more important at high values of E_{rel}, is a direct displacement. The collision energy is transferred to the Li^+–OH_2 intermolecular modes, and the H_2O initially bound dissociates while the attacking H_2O adds and binds. In the second type of dissociation the attacking H_2O binds and after multiple inner turning points the H_2O initially bound dissociates. In future work we plan more quantitative studies of this displacement channel.

V. Recombination Rate Constants

Either the analytic expression for the trajectory recombination cross section or that for the microscopic rate constant can be integrated over the Boltzmann initial relative translational energy distribution to find the thermal recombination rate constant. Using eq 7 for the recombination cross section yields the following for the thermal rate constant and activation energy:

$$k(T) = (\pi\mu)^{-1/2}(2/k_bT)^{3/2}a(b + 1/k_bT)^{-2}$$
$$E_a(T) = k_bT(-3bk_bT + 1)\ 2(bk_bT + 1)^{-1} \tag{9}$$

Similarly, eq 8 for the microscopic recombination rate constant gives

$$k(T) = (1/k_bT)^{-3/2}a'(b' + 1/k_bT)^{-3/2}$$
$$E_a(T) = -3k_bT/2 + 3(b' + 1/k_bT)^{-1}/2 \tag{10}$$

for the recombination rate constant and activation energy.

The trajectory thermal rate constants are given in Figure 4 for $K^+ + H_2O$, $Na^+ + H_2O$, $Li^+ + H_2O$, and $Li^+(H_2O) + H_2O$; and in Figure 5 for $Li^+ + H_2O$, $Li^+ + D_2O$, $Li^+ + (CH_3)_2O'$ and $Li^+ + (CH_3)_2O$. The rate constant in eq 9 is given by the curve marked A, while $k(T)$ in eq 10 is given by the curve marked B. The maximum difference between the two rate constants occurs

(48) In future work, we plan to include the modifications to the ADO theory as proposed by Bates in ref 18 and 19.

(49) Longer lifetimes were not investigated because of the amount of CPU time required for such calculations.

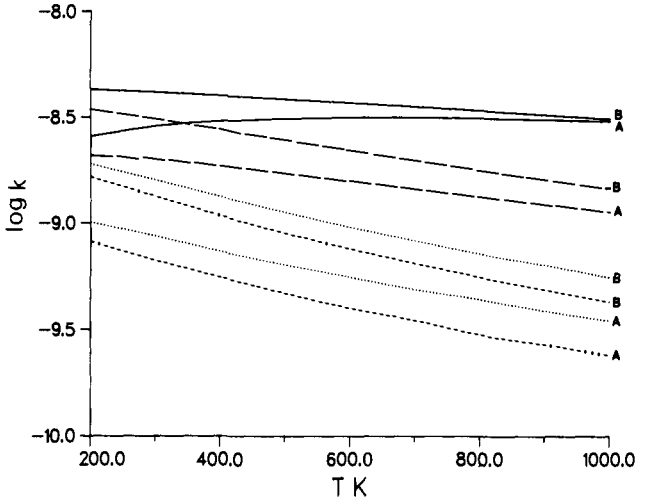

Figure 4. Plot of the base 10 logarithm of $k(T)$ in cm^3/molecule s vs. $T(K)$ for $M^+ + H_2O \rightarrow M^+(H_2O)$: (—) M^+ is $Li^+(H_2O)$, (---) M^+ is Li^+, (· · ·) M^+ is Na^+, and (---) M^+ is K^+. The curves A were calculated with eq 9 and the curves B with eq 10.

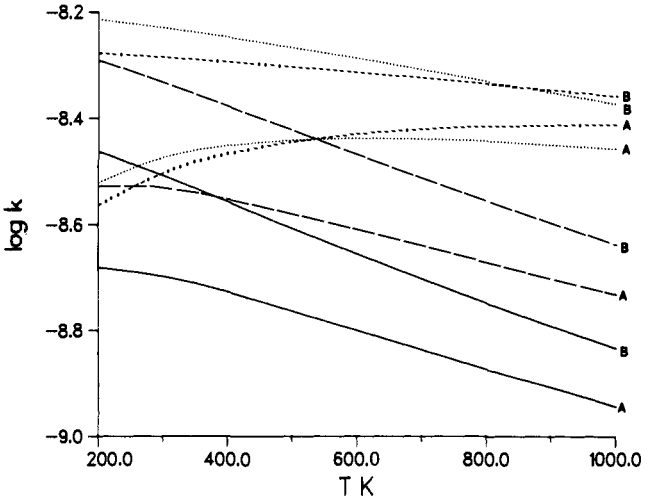

Figure 5. Same as Figure 4 but $Li^+ + M \rightarrow Li^+(M)$: (—) M is H_2O, (---) M is D_2O, (· · ·) M is $(CH_3)_2O$, and (---) M is $(CH_3)_2O'$.

Table VII. Recombination Rate Constants at 300 K[a]

reaction	method: quasiclassical trajectory[b]	ADO theory	AMI theory
$K^+ + H_2O$	1.34	1.60	3.10
$Na^+ + H_2O$	1.60	1.76	3.41
$Li^+ + H_2O$	3.11	2.51	4.88
$Li^+ + D_2O$	4.66	2.48	4.80
$Li^+(H_2O) + H_2O$	4.18	1.74	3.37
$Li^+ + (CH_3)_2O$	5.19	2.27	3.84

[a] Rate constants are given in units of 10^{-9} cm^3/molecule·s. [b] The quasiclassical trajectory rate constants are obtained from eq 10.

at the lowest temperatures. At 300 K the largest difference between the two rate constants is a factor of 2.0 and occurs for $K^+ + H_2O$.

A comparison of the quasiclassical trajectory, ADO, and AMI rate constants at 300 K is given in Table VII. Overall, the three methods give rate constants which agree to within a factor of 2. ADO theory is in the best agreement with the quasiclassical trajectory results for the least efficient recombination reactions, while AMI theory is in the best agreement for the most efficient reactions.

The recombination rate constants could be evaluated more precisely by finding them directly from Monte Carlo quasiclassical trajectory calculations.[34,35] However, this would eliminate calculating the cross sections, a property which provides valuable information about the recombination dynamics.

Table VIII. Recombination Probabilities for $Li^+ + H_2O$ at $b = 0$

E_{rel}[a]	$P_r(E_{rel})$	E_{rel}[a]	$P_r(E_{rel})$
0.25	0.36 ± 0.06	2.00	0.14 ± 0.05
0.50	0.39 ± 0.06	2.50	0.067 ± 0.029
1.00	0.26 ± 0.06	3.00	0.02 ± 0.014
1.50	0.12 ± 0.04		

[a] E_{rel} is in units of kcal/mol.

VI. Recombination Dynamics

The results of this study provide insight into constructing an accurate collisional model for describing ion–molecule recombination. One begins by writing the recombination cross section as

$$\sigma(E_{rel}) = \int_0^{b_m} P_r(E_{rel},b)2\pi b\,db \qquad (11)$$

In parts I and II it was found that the recombination probability, $P_r(E_{rel},b)$, is nearly independent of b in the range 0–b_m for a fixed E_{rel}. As a result a good approximation to the reactive cross section is

$$\sigma(E_{rel}) \simeq \int_0^{b_m} P_r(E_{rel})2\pi b\,db \qquad (12)$$

The trajectory calculations indicate that the probability $P_r(E_{rel})$ is a product of two probabilities: one a geometric or steric probability, and the other an energy-transfer probability.

The effect of the above two probabilities is illustrated in Table VIII where $P_r(E_{rel})$ is given for $Li^+ + H_2O$ trajectory calculations at $b = 0$. If energy transfer is the only necessary criteria for recombination to occur, $P_r(E_{rel})$ is expected to approach unity as E_{rel} goes to zero.[38,39] As shown in Table VIII, this is clearly not the case for $Li^+ + H_2O$ collisions. The origin of this difference is collisions in which Li^+ approaches H_2O at orientations where the Li^+—H repulsions are felt (see potential energy contour in part I).[38] At low initial relative translational energies this repulsive barrier cannot be overcome and the outcome is nonreactive scattering.

At the larger values of E_{rel} the geometric term should be unimportant, and the results in Table VIII and those of parts I and II suggest that the energy transfer probability can be approximated by an exponential. The exact mechanism for energy transfer is not known. Relative translational energy to rotational energy transfer T → R, where orbital angular momentum l is transferred to H_2O rotational angular momentum j, is the most probable initial energy-transfer step. Other possible energy-transfer steps are translation to vibration T → V, and rotation to vibration R → V. Model studies would be useful to delineate these different energy-transfer processes. For example, the three H_2O vibrational frequencies can be uniformly increased to see how the $Li^+ + H_2O$ recombination cross section varies. In the high-frequency limit the only energy transfer mechanism is T → R. An interesting system for comparison is $Li^+ + (CH_3)_2O$ with the $(CH_3)_2O$ frequencies increased to the high-frequency limit and the two internal rotations (IR) treated as free rotors. There there are two energy-transfer mechanisms T → R and T → IR as compared to only T → R for $Li^+ + H_2O$. It would also be interesting to see how the T → R probability for $Li^+ + H_2O$ changes as the H_2O moments of inertia are increased.

The largest impact parameter that leads to recombination in the trajectory calculations at a specific E_{rel} can be identified as the impact parameter for which a minimum still exists in the effective potential energy curve V_{eff} along the minimum energy path.[38,39] A minimum in V_{eff} allows the ion–molecule collision to reach the strong interaction region so that coupling between the intermolecular and molecular degrees of freedom can occur. This is shown in Figure 6 where transitions between different V_{eff} curves is depicted; i.e., $l \rightarrow j$ energy transfer is assumed.

As pointed out above, it is found that the recombination probability $P(E_{rel},b)$ is nearly independent of b in the range 0–b_m

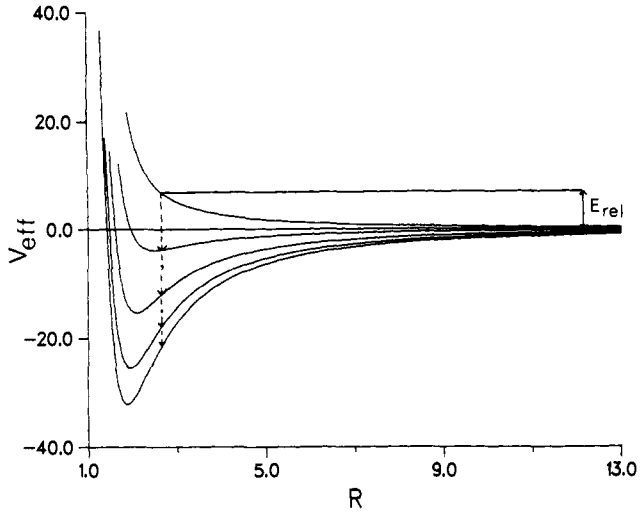

Figure 6. Depiction of ion–molecule recombination by $l \rightarrow j$ angular momentum transfer.

for a fixed E_{rel}. For collisions which occur with small values of b, the dominant energy-transfer mechanism leading to recombination is expected to be T → V. As the value of b for the collision approaches b_m, the T → R process is expected to compete with T → V as a result of the collisional orbital angular momentum. The insensitivity of $P(E_{rel},b)$ to b for $b < b_m$ and E_{rel} a constant indicates that these two energy-transfer processes have similar efficiencies for ion–molecule recombination.

VII. Conclusion

This quasiclassical trajectory study has shown that there are interesting and important dynamical features involved in ion–molecule recombination reactions. Formation of the ion–molecule collision complex requires that the initial relative translational energy be transferred to rotational and/or vibrational degrees of freedom. In order to understand this energy-transfer process, the structure and internal degrees of freedom for both the ion and molecule must be considered.

Only electrostatic intermolecular potentials have been considered in this work. However, the results may have important ramifications for ion–molecule reactions in which chemical bond ruptures and formations take place. In such reactions there are often two important minimia on the potential energy surface.[1-3] One results from the long-range electrostatic interactions. The other is formed by the stronger short-range chemical interactions. It is usually assumed that the ion–molecule complex is first trapped in the long-range minimum, and, after intramolecular energy transfer into the proper internal coordinates occurs, the complex moves into the deeper short-range minimum. This study indicates that for some ion–molecule reactions trapping of the complex in the long-range minimum may be an inefficient process. Thus, the long-range intermolecular potential will not determine the rate of the ion–molecule reaction. Such an effect has been seen in several experimental studies.[50-52] Calculating trajectories on potential energy surfaces which have both the short- and long-range minima is an important research topic for future studies.

Acknowledgment. This research was supported by the National Science Foundation.

Registry No. H_2O, 7732-18-5; K^+, 24203-36-9; Na^+, 17341-25-2; Li^+, 17341-24-1; $(CH_3)_2O$, 115-10-6.

(50) L. Bass, W. J. Chesnavich, and M. T. Bowers, *J. Am. Chem. Soc.*, **101**, 5493 (1979).
(51) J. J. Grabowski, C. H. DePuy, and V. M. Bierbaum, *J. Am. Chem. Soc.*, **105**, 2565 (1983).
(52) R. R. Squires, V. M. Bierbaum, J. J. Grabowski, and C. H. DePuy, *J. Am. Chem. Soc.*, **105**, 5185 (1983).

Bound Pyrene Excimer Photophysics and the Organization and Distribution of Reaction Sites on Silica

C. H. Lochmüller,*† A. S. Colborn,† M. L. Hunnicutt,† and J. M. Harris‡

Contribution from the Paul M. Gross Chemical Laboratory, Duke University, Durham, North Carolina 27706, and the Department of Chemistry, University of Utah, Salt Lake City, Utah 84112. *Received November 14, 1983*

Abstract: A study of the time-dependent luminescence of pyrene silane molecules chemically bound to microparticulate silica was undertaken to determine the distribution of molecules chemically bound to silica and their organization in contact with different solvents. The results indicate that the organization and proximity of such molecules are controlled primarily by an inhomogeneous distribution of chemically reactive silanols on the surface. Analysis of the monomer emission decay profiles at several different surface concentrations indicates that the bound molecules are clustered predominantly into regions of high density. Dynamic, solvent-induced conformation changes of the bound molecules were observed in the excimer and monomer emission decay profiles.

A recent article reported on the steady-state luminescence of pyrene silane molecules chemically bound to silica and suggested that clustering of molecules is significant even at less than 10% of the total attainable surface coverage.[1] The resulting picture of the derivatized surface was one of high-density patches of alkyl ligands in contrast to the uniform and relatively ordered blanket that has been envisionsed in other reports.[2] An understanding of the microscopic organization of chemically modified silica surfaces is of particular importance to separation science, especially if one considers the widespread use of such materials as bonded phases in liquid chromatography. Recent studies provide an improved understanding of the influence of solvent modification of the bonded phase on the solute distribution process in re-

†Duke University.
‡University of Utah.

(1) Lochmüller, C. H.; Colborn, A. S.; Hunnicutt, M. L.; Harris, J. M. *Anal. Chem.* **1983**, *55*, 1344.
(2) Unger, K. K.; Roumeliotis, P. *J. Chromatogr.* **1978**, *149*, 211.

0002-7863/84/1506-4077$01.50/0